

MARIAN BRANNY*

NUMERICAL SIMULATION OF AIRFLOW IN BLIND HEADINGS VENTILATED WITH JET FANS

**SYMULACJA NUMERYCZNA PRZEPŁYWU POWIETRZA W WYROBISKU ŚLEPYM
Z WENTYLATOREM WOLNOSTRUMIENIOWYM**

The paper presents a method of calculation of velocity field in blind galleries ventilated by jet fans. The CFD code was used in numerical prediction of the airflow. Mathematical model consists of equations of continuity, Navier-Stokes and the standard equations of $k-\varepsilon$ model of turbulence. The governing equation system is modified in near-wall region by introducing the wall function. There was assumed that the flow is turbulent, geometrically three-dimensional and the air could be treated as an incompressible gas. There were studied the flow fields obtained for two galleries with different cross-sections. Calculations and *in situ* measurements were performed for galleries in copper mines. The calculated flow field, projected on same horizontal planes is presented. The measurements were taken in four cross-sections of gallery. A rotating vane anemometer and velometer were used in measurements. The experimental results were used to test simulation data. The quantitative correlation between experimental and numerical results is good but there are notified quantitative differences, however the accuracy of numerical representation seems to be sufficient for practical applications. The reasons of above differences stick both in simplifications of theoretical model as well as in measurement technics. The selection of proper boundary conditions on walls (giving consideration to roughness of surfaces) and at inlet is fundamental for accurate predictions.

Key words: underground ventilation, auxiliary ventilation, CFD models, mathematical model

Eksplotacja w kopalniach LGOM-u polega na rozcinaniu złoża pasami i komorami na filary technologiczne. Komory tworzą wyrobiska ślepe o długościach wynoszących przeważnie 25–30 m, które przewietrzane są wentylatorami wolnostrumieniowymi instalowanymi na ich wlotach. Skuteczność przewietrzania zależy od zasięgu strumienia generowanego przez wentylator, a jej ocena może opierać się na istniejącym rozkładzie parametrów takich jak prędkość przepływu, temperatura powietrza czy stężenie gazów.

W artykule przedstawiono teoretyczny sposób wyznaczania pola prędkości w wyrobiskach ślepych przewietrzanych wentylatorami wolnostrumieniowymi oraz w oparciu o pomiary *in situ* podjęto próbę weryfikacji modelu. Do opisu ruchu powietrza w komorze wykorzystano technikę bazującą na metodach CFD. Rozważany przepływ jest typu eliptycznego, można w nim wyróżnić obszar ze strugą

* WYDZIAŁ GÓRNICTWA I GEOINŻYNIERII, AKADEMIA GÓRNICZO-HUTNICZA, 30-059 KRAKÓW, AL. MICKIEWICZA 30

nawiewną, strefę objętą przepływem recyrykulacyjnym i warstwą z przepływem przyściennym. Model matematyczny złożony jest z równań Naviera-Stokesa (1) i ciągłości (2) oraz dwu równań (4), (5) tworzących model lepkości turbulentnej $k-\varepsilon$ (kinetyczna energia turbulencji, dyssypacja kinetycznej energii turbulencji). Warunki brzegowe na ścianach zadawane są w postaci funkcji przyściennych uwzględniających chropowatość powierzchni. Przy formułowaniu równań zachowania opisujących przepływy w warstwie przyściennej korzystano z badań J. Nikuradzego. W rozwiązaniu numerycznym stosowano dwuwarstwowy model funkcji ściany, oparty na równaniach (10) i (11). Naprężenia styczne na ściance chropowej wyznaczano z zależności (12) i (13). W węzłach bezpośrednio przylegających do ścian sztywnych model turbulentny jest modyfikowany poprzez uwzględnienie w równaniu (1) siły powodującej zmniejszanie prędkości w warstwie przyściennej, wynikającej z zależności (12), (13). Również w członach źródłowych równania (4) wprowadza się odpowiednie zmiany uwzględniające naprężenia styczne zdefiniowane wzorami (12), (13).

W rozważaniach przyjmuje się, że przepływ ma charakter turbulentny 3D, a powietrze jest gazem nieciśniliwym. Dyskretyzację obszaru przeprowadzono w oparciu o siatkę różnicową o przesuniętych węzłach. Przy wyprowadzaniu schematu różnicowego korzystano z metody objętości kontrolnej oraz techniki *up wind*. Czlonki konwekcyjne i dyfuzyjne aproksymowano schematem hybrydowym. Do wyznaczania pola prędkości i ciśnień stosowano algorytm (Brann 2000) wzorowany na procedurach SIMPLE/SIMPLER.

Obliczenia i pomiary *in situ* prędkości przepływu powietrza wykonano dla dwóch komór różniących się wymiarami poprzecznymi i polami przekrojów. Kształt i wymiary komór, w których wykonano pomiary przedstawiono na rysunku 1. Wyrobiska przewietrzane były wentylatorami WOO-63. W obliczeniach numerycznych przyjęto, że komory mają kształt prostopadłościów o wymiarach $5,0 \times 2,0 \times 27 \text{ m}$ i $5,5 \times 4,0 \times 26 \text{ m}$. Wyznaczone pola prędkości prezentowane są w postaci rzutów na wybrane płaszczyzny pionowe (x_1-x_3) przedstawione na rysunkach 2 i 3. W obu wariantach strumień powietrza płynie do przodka wzdłuż ścian wyrobiska przy których umieszczony jest wentylator, natomiast strumień powrotny wzdłuż ścian przeciwległych. Strefa wyrobiska roztacząca się od wentylatora na odległość 17–18 m charakteryzuje się intensywnym mieszaniem powietrza. Ilość recyrykulującego powietrza w znacznej jej części przekracza wydatek wentylatora.

Prędkość przepływu powietrza mierzono anemometrem skrzydełkowym firmy Lambrecht, weletem precyzyjnym firmy Luga oraz anemometrem czasowym firmy Castell. Rysunki 4, 5 i 6 przedstawiają rozkłady prędkości (obliczonej i zmierzonej) wzdłuż linii pomiarowych (osi x_2) w trzech wybranych przekrojach poprzecznego komory niskiej. Zmierzone i obliczone maksymalne i minimalne prędkości w odległościach równych 0,5 m od stropu i spagu oraz w połowie wysokości wyrobiska zestawiono w tabeli 1.

Pod względem jakościowym, wygenerowany na drodze numerycznej obraz pola prędkości odzwierciedla przepływ rzeczywisty, odnotowuje się natomiast różnice ilościowe. Przyczyn tych różnic można upatrywać zarówno w uproszczeniach tkwiących w modelu teoretycznym, jak i w technice pomiaru prędkości przepływu. Zależności (12) i (13) uwzględniają tzw. chropowatość piaskową, opierającą się na jednym wymiarze charakterystycznym — wymiarze nierówności ściany. Wiadomo, że wpływ ma nie tylko wysokość nierówności, ale również ich kształt oraz gęstość rozmieszczenia na powierzchni. Wyrobiska górnicze charakteryzują się dużą, niejednorodną chropowatością ścian. Jest to rodzaj przewodów wentylacyjnych nie mający odpowiednika w innych zastosowaniach technicznych. W piśmieństwie brakuje sprawdzonych wzorów uwzględniających wpływ tego typu chropowatości na przepływ w warstwie. Przy stosowanej technice pomiaru wielkością mierzoną był moduł wektora prędkości, natomiast kierunek i zwrot określano wizualnie. Przy tej metodzie błąd pomiaru może być znaczny, szczególnie w obszarach o zmiennym kierunku przepływu.

Pomimo stwierdzonych różnic ilościowych pomiędzy obliczeniami i pomiarami można uznać, że wyniki symulacji numerycznej opisują przepływ rzeczywisty z wystarczającą dla praktyki dokładnością. Dokładność odwzorowania zależy przede wszystkim od wyboru właściwych warunków brzegowych na ścianach sztywnych (uwzględniających dużą chropowatość powierzchni) oraz w otworze nawiewnym.

Słowa kluczowe: wentylacja kopaliń, wentylacja odrębna, modele CFD, model matematyczny

1. Introduction

Mining operations in copper mines in the Legnica-Głogów region employ chiefly the room and pillar method where the deposit is “cross-cut” to form chambers and protecting pillars. The rooms, usually 25–30 m long, are cross-cut parallel to the working face advance. The face zones are ventilated by means of jet fans installed at the inlets. The copper mines in that region obtained the necessary permission from the mining authorities to use this sort of ventilation in blind headings and galleries up to 60 m long. The range of penetration of an air stream generated by the jet fan is determined by several parameters; the major determinants being the initial stream parameters (i.e. diameter, initial velocity and the magnitude of turbulence). When turbulence increases, the process of mass and momentum transfer between the air stream and the ambience is thus intensified and, as a result, velocity measured along the stream axis decreases more significantly and the range of penetration gets smaller. The shape of the emerging velocity field depends on the actual fan location in the heading cross-section. A stream of fresh air may flow along the side wall by which the fan is positioned while the return stream flows along the opposite wall. When the initial energy of the stream is small, it may not reach the face zone at all. In that case a secondary vortex is generated which may embrace the greater section of the aired heading. The shape of the velocity field and hence the intensity of ventilation is affected by the presence of any obstacles the air stream might encounter, such as out-of-straight axis of the gallery, variability of its cross-section or the presence of very rough surfaces (side walls, roof, floor). The regulations currently in force set forth the conditions for jet fan installation and fan operating parameters. These regulations are based on many years' experience as well as results of extensive research work on mechanisms of air stream flows (Biernacki 1975; Rosiek et al. 1993; Sułkowski et al. 1998, 1999, 2000).

The aim of this study is to find the velocity field in a blind heading ventilated by a jet fan in the theoretical approach and to check how accurately the predicted velocity field should embody the real flow by way of measurements in situ. Parameters characterising airflow in the chambers were determined with the use of a technique based on CFD models, widely employed now in industrial applications. CFD models involve numerical solving of systems of differential equations of continuity, momentum and energy conservation, affording us the distributions of velocity, pressure, temperature and concentration of chemical species within the aired region. Airflow within the heading is of elliptical type with three distinct zones: the inlet stream zone, the zone with recirculation flow and the near-wall region. To solve directly the equations describing turbulent flows requires that a very fine grid be used (in our case 10^{14}), which in fact would preclude the use of this procedure. In order to overcome this drawback, the turbulent models are employed which require less fine grids. The turbulence models appear to complete the basic sets of fluid mechanics equations. Depending on the applied averaging procedure, we get the model of turbulent viscosity and Reynolds stress model (time-averaging) or the large eddy simulation model (*LES*) where space averaging is utilised. This study makes use of the two-parameter model $k-\varepsilon$ (kinetic

energy of turbulence — dissipation rate of turbulent kinetic energy). This model has most widespread applications and has been already used to investigate flows in mines (Branny 2000; Gao et al. 2001) or in large-sized structures (Beghein et al. 1994; Borth, Suter 1994; Lipska 1997a, b).

2. Mathematical model

The assumptions are made that airflow in a blind heading is steady and air is an incompressible gas. Turbulent flows are described with the system of equations including the Navier-Stokes equations (1) and the equation of continuity (2):

$$\frac{\partial(u_i u_j)}{\partial x_j} - \frac{\partial}{\partial x_j} \left(v_{ef} \frac{\partial u_i}{\partial x_j} \right) = -\frac{1}{\rho} \frac{\partial}{\partial x_i} \left(p + \frac{2}{3} k \rho \delta_{ij} \right) + \frac{\partial}{\partial x_j} \left(v_{ef} \frac{\partial u_j}{\partial x_i} \right) \quad (1)$$

$$i, j = 1, 2, 3$$

$$\frac{\partial u_i}{\partial x_i} = 0 \quad (2)$$

where:

- u_i — averaged velocity vector component in the i -th direction,
- ρ — air density,
- $v_{ef} = v + v_T$,
- v, v_T — denote the molecular and turbulent velocity, respectively,
- k — kinetic energy of turbulence,
- p — averaged static pressure,
- δ_{ij} — Kronecker delta.

In the $k-\varepsilon$ model the turbulent viscosity is obtained from the formula:

$$v_T = C_\mu \frac{k^2}{\varepsilon} \quad (3)$$

where:

- C_μ — model constant,
- ε — dissipation rate of kinetic energy of turbulence.

The kinetic energy of turbulence k and the rate of kinetic energy dissipation ε are derived from the transport equations (4) and (5).

$$\frac{\partial(u_j k)}{\partial x_j} - \frac{\partial}{\partial x_j} \left\{ \left(v + \frac{v_T}{\sigma_k} \right) \frac{\partial k}{\partial x_j} \right\} = v_T \frac{\partial u_j}{\partial x_i} \left(\frac{\partial u_i}{\partial x_j} + \frac{\partial u_j}{\partial x_i} \right) - \varepsilon \quad (4)$$

$$\frac{\partial(u_j \varepsilon)}{\partial x_j} - \frac{\partial}{\partial x_j} \left\{ \left(v + \frac{v_T}{\sigma_\varepsilon} \right) \frac{\partial \varepsilon}{\partial x_j} \right\} = C_1 \frac{\varepsilon}{k} v_T \frac{\partial u_j}{\partial x_i} \left(\frac{\partial u_i}{\partial x_j} + \frac{\partial u_j}{\partial x_i} \right) - C_2 \frac{\varepsilon^2}{k} \quad (5)$$

where:

$C_1, C_2, \delta_k, \delta_e$ — model constants.

When fluid incompressibility being assumed, eq (1)–(5) constitute a complete system of equations. The model $k-\varepsilon$ introduces five empirical quantities $C_\mu, C_1, C_2, \delta_k, \delta_e$ which are treated as constants in actual solutions. When the turbulent number $Re = \frac{k^2}{\varepsilon v}$ exceeds 400, several authors would assume that $C_\mu = 0.09, C_1 = 1.44, C_2 = 1.9,$

$\delta_k = 1.0, \delta_e = 1.3$ (Lauder, Spalding 1972; Beghein et al. 1994; Gao et al. 2001).

Equations (3), (4) and (5) make up the model $k-\varepsilon$ for large Reynolds numbers where viscous interactions are ignored though they may be of paramount importance in near-wall regions. In near wall regions where turbulent Reynolds number is small, molecular viscosity decidedly affects the process of generation, dissipation and transport of turbulent features. That is why certain model modification would be required to incorporate the regions near the solid walls that limit the flow.

2.1. Boundary conditions

The boundary conditions are:

- on solid walls:

$u_i = 0$ — no-slip flow condition

$$\frac{\partial p}{\partial n} = 0 \quad (6)$$

where:

n — coordinate perpendicular to surface,

while k and ε are obtained from the modified turbulence model for near wall regions (Lauder, Spalding 1972; Kolniak et al. 1983);

- in the inlet cross-section:
 u_i, k and ε are given in the form of Dirichlet's conditions;
- in the outlet cross-section:
in the flow direction x_1

$$\frac{\partial u_i}{\partial x_1} = \frac{\partial k}{\partial x_1} = \frac{\partial \varepsilon}{\partial x_1} = 0 \quad p = 0 \quad (7)$$

Here pressure is relative variable, not an absolute one. The reference pressure is set on outlet cross-section. The reason is that the value of absolute pressure is much larger than its local differences that are encountered in finite difference method. Setting $p = 0$ as a relative value helps us to keep down the round-off error in numerical calculation.

This conditions are fulfilled as long as the flow is fully developed. To simplify the numerical procedure (i.e. to reduce the number of nodes) the boundary embodying the conditions on the outlet cross-section is located in the region where the flow is not fully developed yet though the flow direction is determined, there is no return flow and it is sufficiently far from the zone being the subject matter of the study. Thus formulated condition is formally correct and it affects the results of computations only in a minor degree.

2.2. Modification of the turbulence model for the near-wall region

In the vicinity of solid walls limiting the flow we observe large velocity variations: from zero on wall surfaces up to the value nearing the velocity of an undisturbed stream. Velocity decrease in the boundary layer is the result of fluid viscosity. As the layer is rather thin, the flow is mostly parallel to the wall surface. That is why derivatives of velocity in the direction normal to the wall surface have a greater value than those computed in the direction parallel to the wall. This property is utilised when equations describing flow in boundary zones are formulated. In a two-layer wall function model the zone directly adjacent to solid walls is divided in two regions: the viscous sub-layer stretches from wall up to the distance y_p where $y_+ = C_\mu^{1/4} k^{1/2} y_P / v \leq 11.63$. Stresses in this region are derived from the formula:

$$\tau = \mu \frac{u_P}{y_P} \quad (8)$$

The index P denotes the value in the node directly adjacent to the wall. Beyond that zone, the flow is taken to be turbulent. Accordingly, stresses are obtained from the formula:

$$\tau = u_P \frac{\kappa \rho C_\mu^{1/4} k_P^{0.5}}{\ln \left(\frac{E \Delta n C_\mu^{1/4} k_P^{0.5}}{v} \right)} \quad (9)$$

where:

κ — Karman constant,

E — a constant in the wall function model,

Δn — distance between the point P and the wall.

These relationships are based on the assumption that wall surface is sufficiently smooth. In the case of rough surfaces the formulas have to be modified. According to Nikuradze, the region close to a rough wall is to be divided in three zones; there are

formulas describing the two of these- zone I and III. No formula is available for the transition zone II. In the zone I, nearest the rough surface the velocity distribution is given by the formula:

$$\frac{u}{u_\tau} = 2.5 \ln \frac{du_\tau}{v} + 5.5 \quad (10)$$

where:

d — height of the surface unevenness,

$u_\tau = \sqrt{\tau/\rho}$ — friction velocity.

The formula (10) is applicable for $\frac{du_\tau}{v} < 3$. When $\frac{du_\tau}{v} > 60$, then

$$\frac{u}{u_\tau} = 8.48 \quad (11)$$

The transition zone covers the range $3 < \frac{du_\tau}{v} < 60$.

In the numerical solution utilising the two-layer model based on (10) and (11) the limit point is $u^+ = y_+ = 3$. Shear stress on the rough wall is obtained from the formula:

- for $y_+ = C_\mu^{0.5} k_P d/v < 3$

$$\tau = u_P \frac{\kappa \rho C_\mu^{1/4} k_P^{0.5}}{\ln \left(\frac{E d C_\mu^{1/4} k_P^{0.5}}{v} \right)} \quad (12)$$

- for $y_+ = C_\mu^{0.5} k_P d/v > 3$

$$\tau = \frac{\rho u_P^2}{71.91} \quad (13)$$

The analysis of (12) and (13) leads us to the following conclusions:

When the ratio of d to the viscous layer thickness y_0 is less than 0.25 ($d/y_0 < 0.25$), then surface roughness will not affect velocity distribution in that layer and the surface is treated as smooth. When $d/y_0 > 6$, the effects of surface roughness are significant. Walls in mine headings are highly rough which exceeds the specified value. The flow around such uneven and rough walls must be turbulent. In the zone where the mechanism of turbulent mixing is fully developed, the velocity distribution is approximated (with logarithmic precision) by the following equation (Landau, Lifszyc 1994):

$$\frac{u}{u_\tau} \approx \frac{1}{\kappa} \ln \frac{yu_\tau}{v} \quad (14)$$

Flow velocity in the stream along the rough surface is small. It is approximated that at the distance $y \sim d$ it is of the same order of magnitude as the friction velocity u_τ . Making use of $v/u_\tau = d$ in (14), we get:

$$\frac{u}{u_\tau} \approx \frac{1}{\kappa} \ln \frac{y}{d} \quad (15)$$

Equation (15) provides an approximate description of velocity distribution near a rough surface. It should include one more coefficient (under logarithm sign) whose value is established experimentally.

When the notion of average velocity is utilised, the stress due to friction on a rough heading surface in 1D flows is derived from the formula:

$$\tau = \alpha u_{sr}^2 \quad (16)$$

where:

α — friction factor,

u_{sr} — average flow velocity in the gallery.

The friction factor in copper mines of the Legnica and Głogów region is taken to be of the order of one hundredth Ns^2/m^4 . Introducing the friction velocity into (16), after necessary transformations we get:

$$\frac{u_{sr}}{u_\tau} = \frac{1}{\sqrt{\alpha/\rho}} \quad (17)$$

Comparison of (11) and (17) clearly indicates that the friction factor corresponding to the value 8.48 is 0.017 Ns^2/m^4 . The use of (17) to find the shear stress on walls when the flow direction cannot be precisely determined (i.e. in blind headings) may give rise to certain doubts. However, in Author's opinion, it allows some unknown, empirical quantities to be approximated.

2.3. Numerical procedure

The equations are discretised over a staggered differential grid (Patankar 1980). Pressure, kinetic energy of turbulence, dissipation rate of turbulent kinetic energy and turbulent viscosity are defined in the basic grid nodes while velocity vector components are defined in the nodes located midway between the basic ones. The differential procedure is based on the control volume method (Patankar 1980; Kazimierski 1992; Kolniak et al. 1983) and the *up wind* technique. The convection and diffusion terms are approximated with the hybrid scheme. Velocity and pressure fields are found with the

use of an algorithm (Brann 2000) similar to the SIMPLE/SIMPILER procedure. The systems of algebraic equations are solved using the TDMA method.

3. Numerical simulation of airflow in a blind gallery

Jet fans ventilating blind galleries are located at the inlets. To ensure their best performance they are often installed in corners, near the roof and one of the side walls. Extensive calculations and measurements in situ of airflow velocity were performed in two galleries differing in geometry and cross-section areas. The geometry and dimensions of the two galleries are shown in Fig. 1. The galleries are ventilated with fans WOO-63, their axis being parallel to that of the gallery. Airflow velocity measured at the fan outlet was 40 m/s; the diffuser cross-section area was 0.2 m². The assumption is made in numerical computations that galleries are shaped like rectangular prisms 5.0 × 2.0 × 27 m in size (in the mine Polkowice-Sieroszowice) and 5.5 × 4.0 × 26 m (in the mine Rudna). The fan WOO-63 is located 1 m from the side wall and 0.75 m from the roof in the low chamber (Fig. 1a) and at the distance of 1m from the roof in the higher chamber (Fig. 1b). The numerical solution utilises a heterogeneous grid 150 × 38 × 32 nodes, hence the average size of the elementary cell would be 0.25 × 0.15 × 0.13 m. At the initial stage a coarser grid was used (76 × 20 × 17 nodes). As soon as the adequate level of accuracy was achieved (i.e. the maximal absolute value of divergence for each cell would equal 0.01 s⁻¹), a grid with a doubled number of nodes would be employed. The computation procedure was interrupted when the maximal value of divergence would be less than 0.001 s⁻¹. To check the stability of the solution, the maximal variations of relevant parameters in the nodes admissible in subsequent iterations were determined and volumetric flow rates in heading cross-sections were calculated. In the nodes directly adjacent to solid walls, the turbulent model is slightly modified (1) as it takes into account the force responsible for reduction of airflow velocity in the boundary layer, this force being derived from (12) and (13). Other terms of the equation (4) are also modified to take into account shear stresses defined by (12), (13).

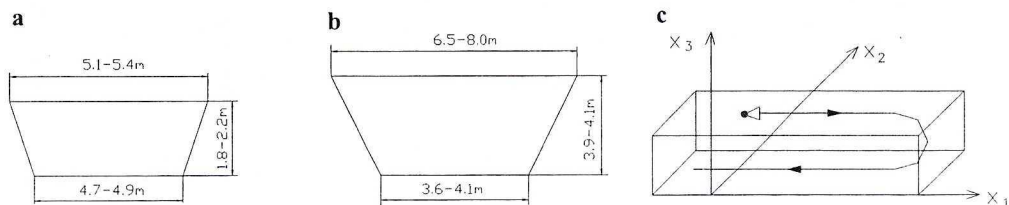


Fig. 1. Scheme of chamber

a) cross-section for chamber from Polkowice-Sieroszowice mine; b) cross-section for chamber from Rudna mine; c) scheme and coordinate system used in numerical simulation

Rys. 1. Schemat komory

a) przekrój poprzeczny komory z kopalni Polkowice-Sieroszowice; b) przekrój poprzeczny komory z kopalni Rudna; c) schemat i układ współrzędnych wykorzystywany w symulacji numerycznej

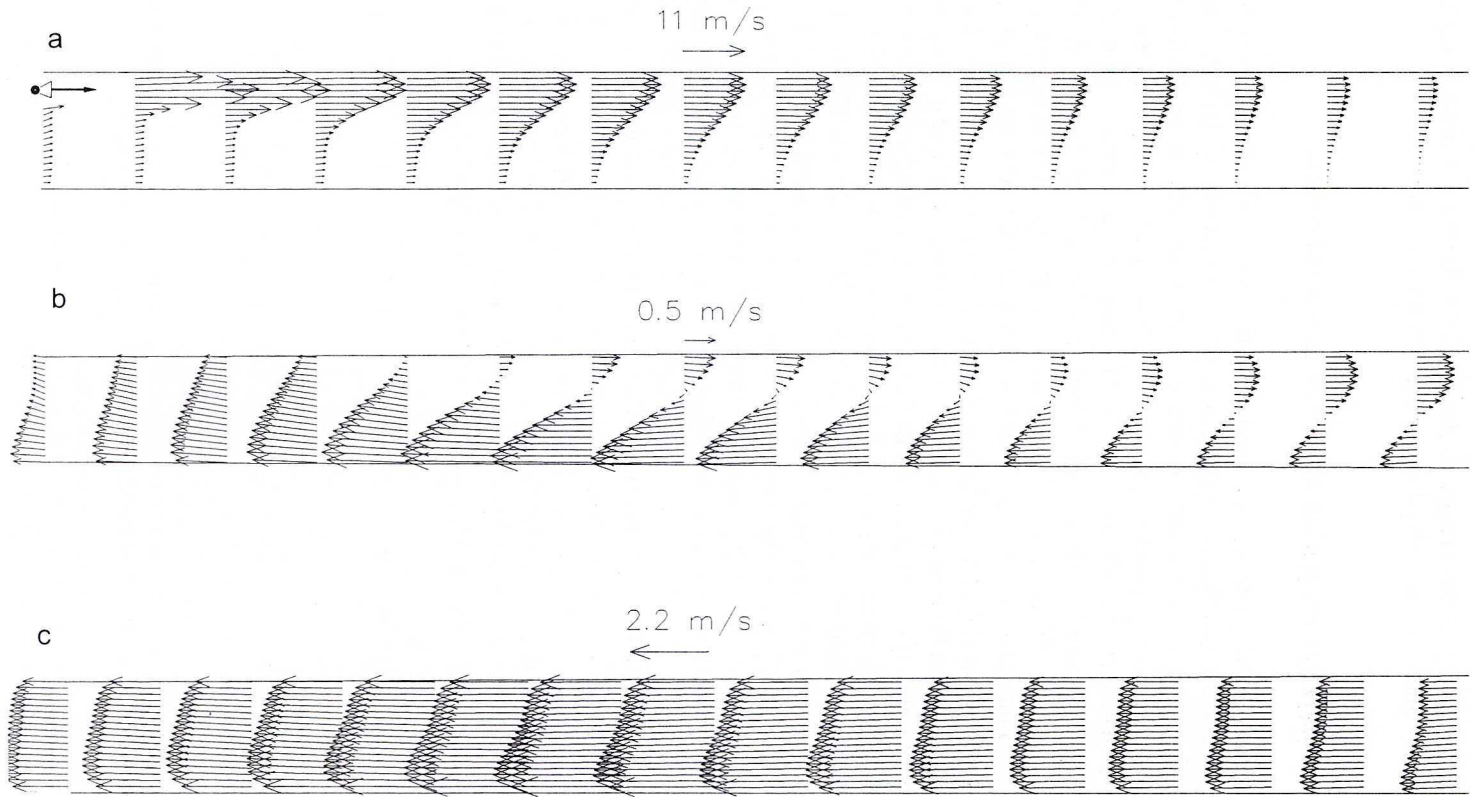


Fig. 2. Velocity field projected on x_1-x_3 plane for low chamber (Fig. 1a)
 a) $x_2 = 4$ m; b) $x_2 = 2.5$ m; c) $x_2 = 1$ m

Rys. 2. Pole prędkości w rzucie na płaszczyznę x_1-x_3 dla komory niskiej (rys. 1a)
 a) $x_2 = 4$ m; b) $x_2 = 2.5$ m; c) $x_2 = 1$ m

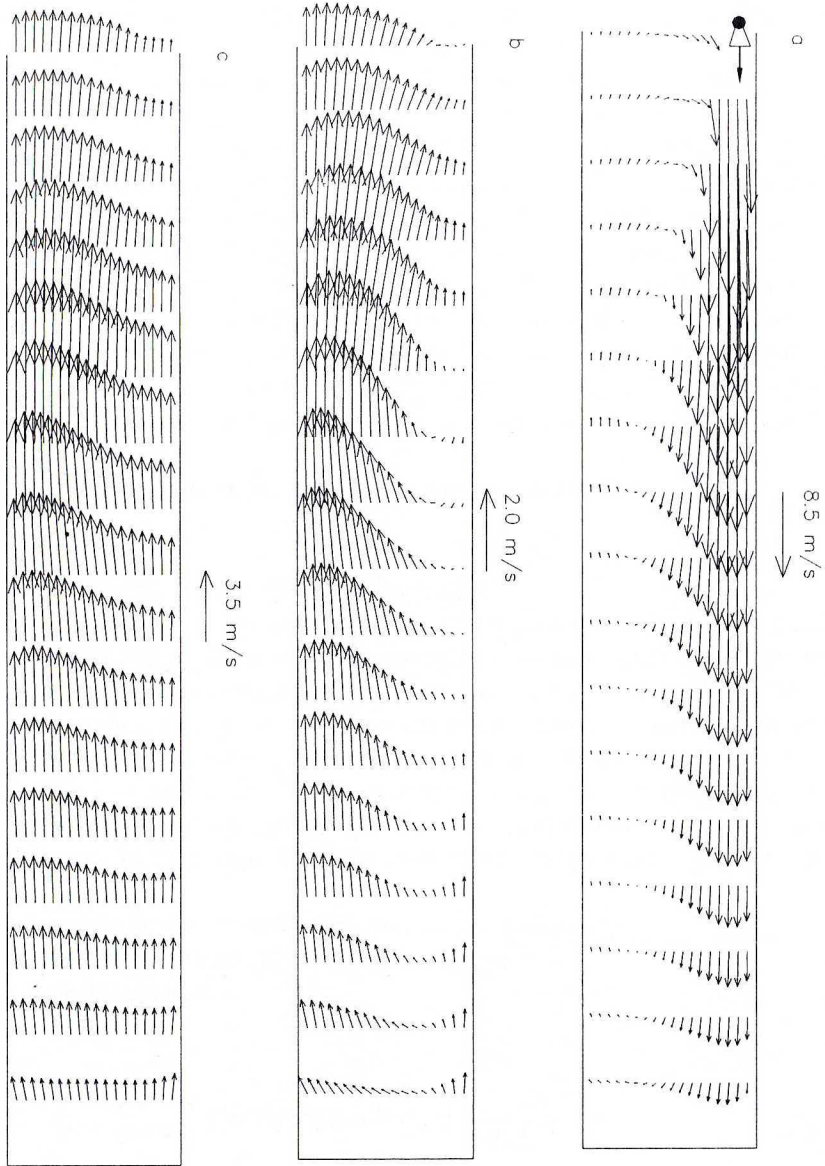


Fig. 3. Velocity field projected on x_1 - x_3 plane for high chamber (Fig. 1b)

b) $x_2 = 4.4$ m, b) $x_2 = 2.75$ m, c) $x_2 = 1$ m

Rys. 3. Pole prędkości w rzucie na płaszczyznę x_1 - x_3 dla komory wysokiej (rys. 1b)
 a) $x_2 = 4.5$ m; b) $x_2 = 2.75$ m; c) $x_2 = 1$ m

Thus obtained velocity fields projected onto the specified vertical planes (x_1-x_3) are shown in Fig. 2 and 3. In both cases the air stream flows towards the face zone, along the wall by which the fan is positioned. The return stream flows along the opposite wall. The amount of air flowing towards the working face zone is obtained from the formula:

$$Q_i = \sum_k \sum_j (|u_1(i,j,k)| + u_1(i,j,k)) \frac{\Delta S(i,j,k)}{2} \quad (18)$$

where:

- i, j, k — node designations,
- u_1 — velocity component in the direction of x_1 -axis,
- $\Delta S(i,j,k)$ — surface area of the elementary cell wall in the plane x_2-x_3 .

In the early stage of stream development the flow rate given by (18) increases. The maximal amount of air passes in the stream cross-section at the distance of 7–8 m from the diffuser outlet and it is three times greater than the fan delivery. At the distance of 17–18 m from the fan, the volumetric flow rate of the stream passing towards the face zone equals the fan delivery. It is the zone of most intensive air mixing. In a greater part of that zone the amount of recirculating air exceeds the fan delivery. Differences in velocity distributions shown in Fig. 2 and 3 are mostly the result of different sizes and cross-sections of the galleries. Maximal air velocities 2 m from the face zone are 3.2 m/s (in the low chamber) and 2.8 m/s (in the higher chamber).

4. Comparison of predicted and measured results

In order to answer the question how accurately the velocity field would embody the real flows, we have to compare the predicted values with measurement results. Measurements were taken in the mines Polkowice-Sierszowice (Fig 1a) and Rudna (Fig 1b). Airflow velocity was measured with a vane anemometer (Lambrecht), providing for digital readout of instantaneous and averaged velocity in the range 0.2–20 m/s; a high-precision velometer (Luga) equipped with extra units for measurements over the range 0–2 m/s and 2–10 m/s and a cup anemometer (Castell). Geometric parameters of the considered headings were measured with the use of a laser range finder. Measurements were taken in heading cross-sections, at the distance of 10 m, 15 m and 20 m from the fan as well as at the distance of 2m from the working face. In each case more than ten measurement points were set along three (chamber in Fig. 1a) or four control lines (chamber in Fig. 1b). The flow direction — the direction and sense of the velocity vector — was determined visually, with the use of a thread indicator. In the course of measurements major flow instabilities were revealed in the shape of reported significant velocity fluctuations. Fig. 4, 5, 6 show predicted and measured velocity distributions along the control lines (the axis x_2) in the three selected cross-sections in the low chamber. The magnitudes of velocity vectors are indicated only as the sign (direction)

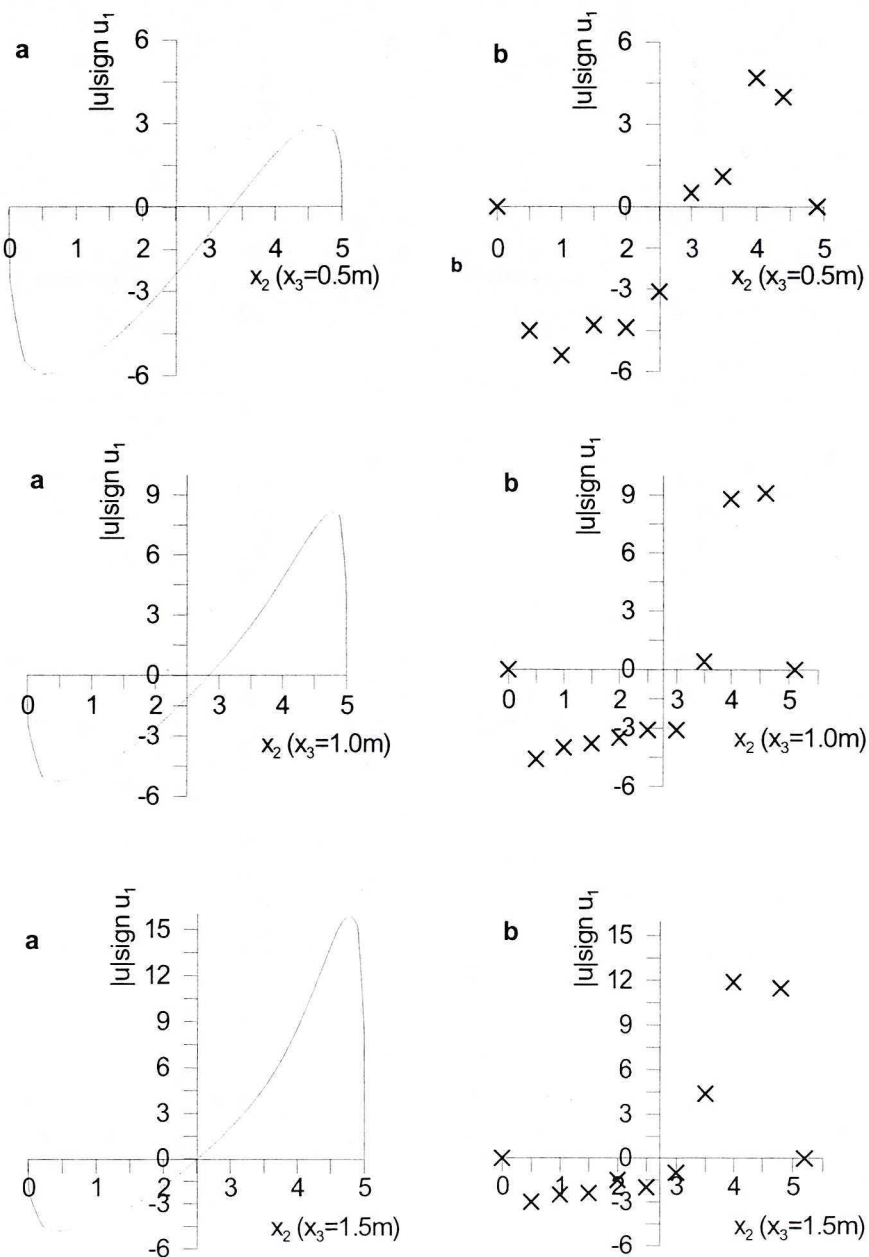


Fig. 4. Distribution of air velocity along x_2 axis (measurement line) for low chamber at a distance 10 m from the fan and 0.5 m, 1.0 m and 1.5 m from the floor
 a) prediction; b) experimental data

Rys. 4. Rozkład prędkości wzdłuż osi x_2 (linii pomiarowej) w komorze niskiej w odległości 10 m od wentylatora oraz 0,5 m, 1,0 m i 1,5 m od spagu
 a) obliczenia; b) pomiary

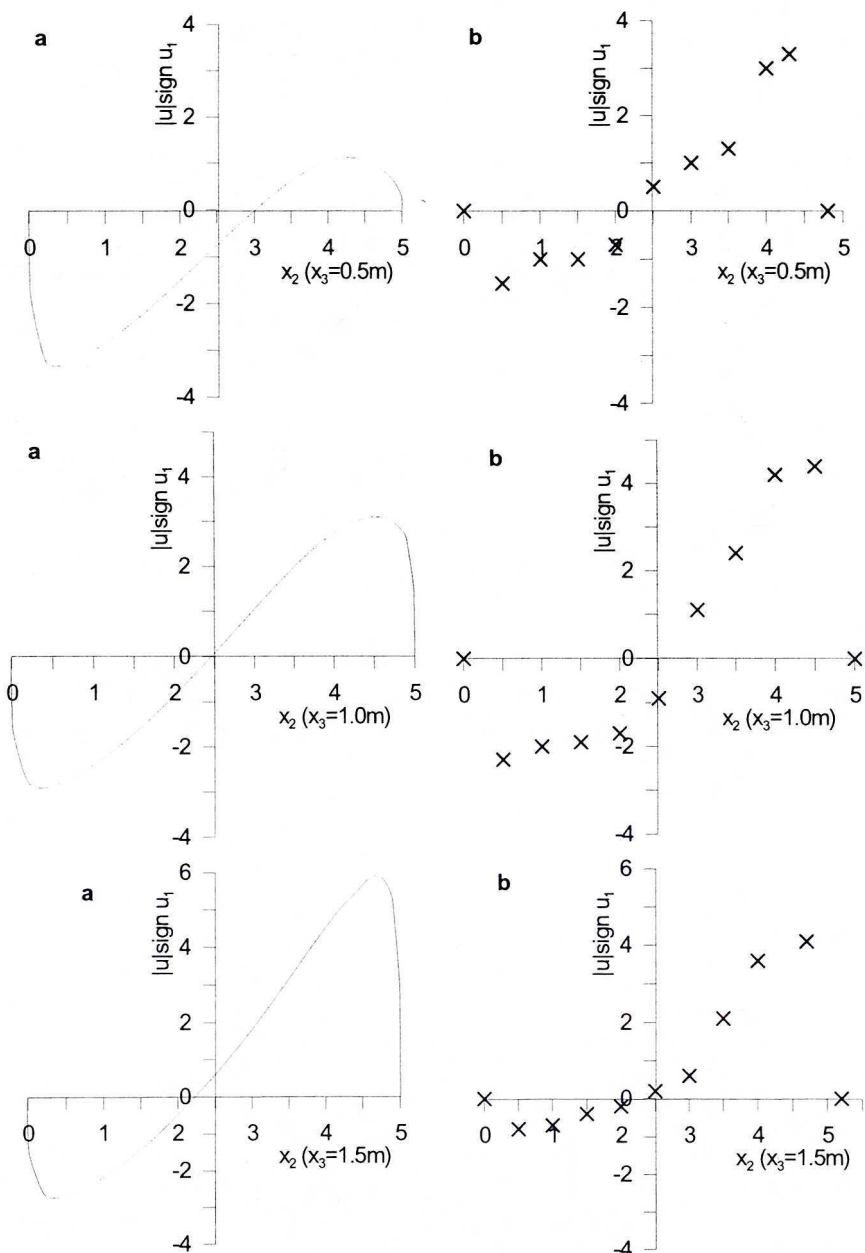


Fig. 5. Distribution of air velocity along x_2 axis (measurement line) for low chamber at a distance 20 m from the fan and 0.5 m, 1.0 m and 1.5 m from the floor
 b) prediction; b) experimental data

Rys. 5. Rozkład prędkości wzdłuż osi x_2 (linii pomiarowej) w komorze niskiej w odległości 20 m od wentylatora oraz 0,5 m, 1,0 m i 1,5 m od spagu
 b) obliczenia; b) pomiary

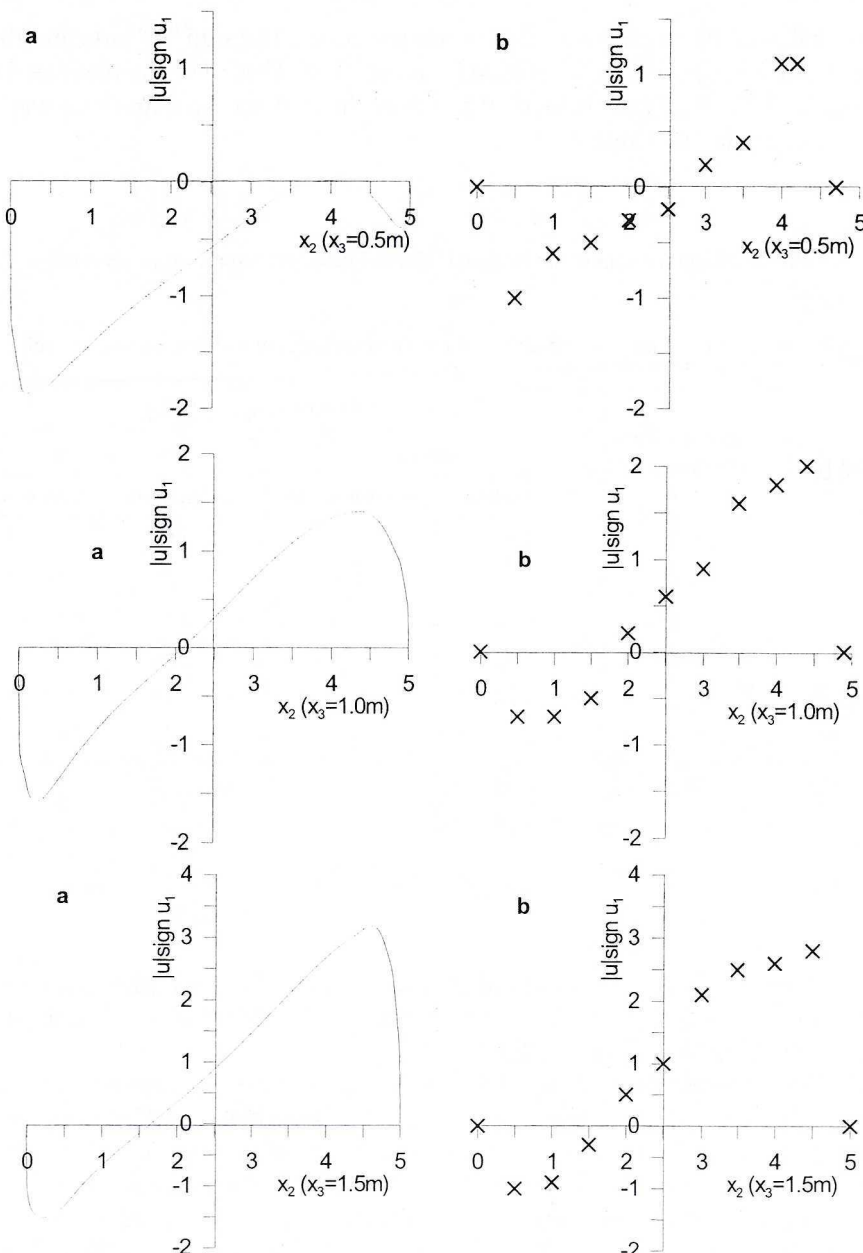


Fig. 6. Distribution of air velocity along x_2 axis (measurement line) for low chamber at a distance 25 m from the fan and 0.5 m, 1.0 m and 1.5 m from the floor
 c) prediction; b) experimental data

Rys. 6. Rozkład prędkości wzdłuż osi x_2 (linii pomiarowej) w komorze niskiej w odległości 25 m od wentylatora oraz 0,5 m, 1,0 m i 1,5 m od spagu
 c) obliczenia; b) pomiary

depends on that of the lengthwise velocity component u_1 . The sign “+” indicates the flow towards the face region whilst “–” is used for return flow. Predicted and measured values of minimal and maximal flow velocity 0.5 m from the roof and floor and half-way up the gallery are compiled in Table 1.

TABLE I

Predicted and measured maximal and minimal velocity in some cross-section

TABELA I

Obliczone i zmierzone maksymalne i minimalne prędkości w wybranych przekrojach

Distance from the fan [m]	Distance from the floor [m]	Velocity $ u \text{sign} u_1$ [m/s]			
		maximal		minimal	
		calculation	measurements	calculation	measurements
10	0.5	2.94	4.7	-5.92	-5.4
	1.0	8.13	8.8	-5.24	-4.6
	1.5	15.86	11.9	-4.79	-3.0
20	0.5	1.11	3.3	-3.31	-1.5
	1.0	3.10	4.4	-2.88	-2.3
	1.5	5.92	4.1	-2.68	-0.8
25	0.5	0.01	1.1	-2.67	-1.0
	1.0	1.39	1.8	-1.87	-0.7
	1.5	3.18	2.8	-1.51	-1.0

Fig. 7 shows the flow velocities predicted and measured in the higher chamber along the control line (axis x_2) set half way up the gallery (2.0 m from the floor), at the distance of 10 m, 20 m and 24 m from the fan.

In qualitative terms the velocity field generated by means of numerical techniques does embody the real flow features, though the quantitative differences are quite significant. There might be several reasons for this state of affairs: simplifications of the theoretical model and inaccuracies involved in flow velocity measurements.

The accuracy of real flow representation depends chiefly on whether the boundary conditions are correctly formulated (Beghein et al. 1994; Lipska 1997a, b.). Flow velocity in the inlet opening was set on the basis of measurements while the kinetic energy of turbulence and the dissipation rate of turbulent kinetic energy were obtained from the predetermined scale of turbulence and the relationship between k , ε and the mixing length in the free stream. Boundary conditions in the outlet cross-section were set in the plane normal to the heading axis, at the distance of 13 m from the fan. In real conditions the fan is positioned at the junction of the chamber and the heading with

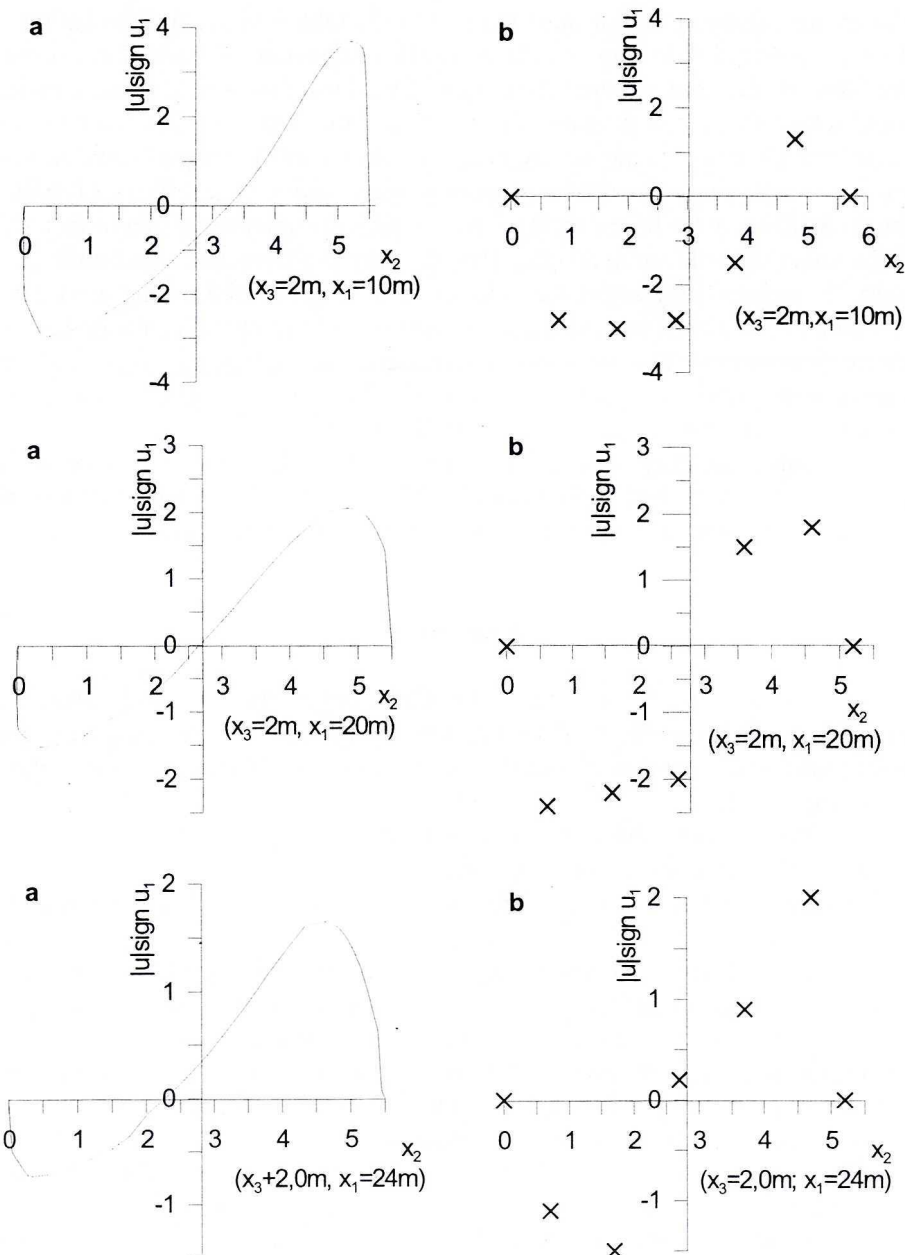


Fig. 7. Distribution of air velocity along x_2 axis (measurement line) for high chamber at a distance 2 m from the floor and 10 m, 20 m and 24 m from the fan
 d) prediction; b) experimental data

Rys. 7. Rozkład prędkości wzdłuż osi x_2 (linii pomiarowej) w komorze wysokiej w odległości 2 m od spagu oraz 10 m, 20 m i 24 m od wentylatora
 d) obliczenia; b) pomiary

circulatory air stream. Relationships (12) and (13) take into account so called “sand roughness” — a feature having one characteristic dimension — the wall unevenness. It is a well-known fact that not only the height of wall roughness is of some importance, but their actual shape and distribution, too. Walls in most mine headings are highly rough and these features being mostly irregular. They form a group of ventilation ducts having no counterparts in other engineering applications. The effects of such wall roughness on flows in the boundary layer are not well documented in literature and ready made formulas are still not available. That the way the boundary conditions on solid walls are formulated may affect the velocity field is confirmed by the work (Branny 2002), which was aimed to reproduce the airflow in the chamber 60 m long using numerical procedures. The velocity field pattern resembling the measured one in qualitative terms (Sułkowski et al. 1998, 1999, 2000) was obtained for $u_s/u_\tau = 3.5$, that is when the friction factor was $\alpha = \approx 0.08 \text{ Ns}^2/\text{m}^4$.

The measured quantity was the absolute value of the velocity vector while its direction and sense were established visually. The error involved in this method may be considerable, particularly in the regions where flow direction should change.

5. Conclusions

The computation technique utilising the CFD method is likely to become a most useful tool for solving mine ventilation problems. Specific difficulties involved in the method application to studies of ventilation strategies in blind headings ventilated by fans have their roots in:

- geometric irregularities of chamber and gallery shape,
- very rough walls of the modelled object,
- most complex velocity fields (presence of zones where major gradients of flow parameters are encountered).

To embody such flow conditions requires that a very fine grid be used. The grid dimension considered in this study is a trade-off between the required accuracy and the costs involved (computer memory and the time expended on computations).

Despite quantitative differences between the predicted and measured values, we are right to suppose that results of computer simulations capture the real flow features with sufficient precision for most practical applications.

Extensive observations have revealed that any obstacles to the air flow generated by the fan (such as rock shelves, uneven walls and roof, the vibrations of the fan or its axis position with respect to the axis of the heading) strongly affect the velocity field pattern. Numerical experiments (Lipska 1997a, b; Branny 2002) indicate that simulations results depend on the way the boundary conditions are formulated. Utmost care must be taken, therefore, to predetermine the right boundary conditions on solid walls and at the inlet.

REFERENCES

- Beghein C., Allard F., Limam K., 1994: Numerical study of the influence of inlet velocity and thermal and solutal diffusivities on air flow pattern in a ventilated enclosure. Fourth International Conference "Roomvent", Kraków, 15–17 June, 123–136.
- Biernacki K., 1975. Wentylator swobodny jako ujemny regulator rozpylu powietrza w sieci. Rozprawa doktorska, Gliwice (niepubl.).
- Borth J., Suter P., 1994. Influence of mesh refinement on the numerical prediction of turbulent air flow in rooms. Fourth International Conference "Roomvent", Kraków, 15–17 June, 137–148.
- Branny M., 2000. Rozkład prędkości, temperatury i koncentracji gazów w komorach oraz strefach przedkowych wyrobisk z wentylacją odrębną. Rozpr. Monografic 91, AGH, Uczel. Wyd. Nauk.-Dydakt., Kraków.
- Branny M., 2002: Analiza pola prędkości w wyrobiskach ślepych z wentylatorami wolnostrumieniowymi. 2 Szkoła Aerologii Górniczej, Zakopane, 7–11 października, 27–36.
- Gao J., Kenichi U., Inoue M., 2001: Simulation of the heat and moisture transfer between airway walls and mine air at a heading face with forcing auxiliary ventilation system. Proc. 7th Int. Mine Vent. Congress, Kraków.
- Kazimierski Z., 1992: Numeryczne wyznaczanie trójwymiarowych przepływów turbulentnych. Wyd. PAN, Wrocław–Warszawa–Kraków, 18–38.
- Kolniak P., Przekwas A., Wanik A., 1983: Metoda modelowania przepływów recyrkulacyjnych. Prace Nauk. Inst. Techn. Cieplnej i Mech. Płyn. Politechniki Wrocławskiej, Monografia 8.
- Landau L.D., Lifszyc E.M., 1994: Hydrodynamika. PWN, Warszawa, 219–223.
- Launder B., Spalding D., 1972: Mathematical models of turbulence, Londyn, Acad. Press.
- Lipska B., 1997a: Kompleksowe badania przepływu powietrza wentylacyjnego w hali sportowej w Monachium. Piąte Ogólnopolskie Sympozjum „Zastosowanie mechaniki płynów w inżynierii środowiska”, Gliwice–Wisła, 185–198.
- Lipska B., 1997b: Rezultaty badawcze ANNEKSU 26 IEA w zakresie prognozowania przepływów wentylacyjnych. Piąte Ogólnopolskie Sympozjum „Zastosowanie mechaniki płynów w inżynierii środowiska”, Gliwice–Wisła, 199–213.
- Patankar S., 1980: Numerical heat transfer and fluid flow. Hemisphere, McGraw-Hill.
- Rosick F., Sikora M., Strumiński A., Urbański J.: Zastosowanie wentylatorów wolnostrumieniowych do wspomagania wentylacji wyrobisk górniczych. Prace Naukowe Instytutu Górnictwa Politechniki Wrocławskiej nr 70, Seria Monografic nr 33.
- Scholtz R., Hanel B., 1998: Computergestützte berechnung der raumlufströmung. Berlin, VEB Verlag Technik.
- Sułkowski J., Frycz A., Drenda J., Biernacki K., Domagała L., 1998: Ocena skuteczności przewietrzania ślepych wyrobisk eksploatacyjnych o długości powyżej 30 metrów przy wykorzystaniu wentylatorów wolnostrumieniowych typu WOO-63. Gliwice (niepubl.).
- Sułkowski J., Drenda J., Biernacki K., Domagała L., 1999: Opracowanie wytycznych stosowania wentylatorów wolnostrumieniowych do przewietrzania drążonych przedków o długości do 60 metrów. Gliwice (niepubl.).
- Sułkowski J., Drenda J., Biernacki K., Gumiński A., Różański Z., Wierzbiński K., Musioł D., 2000: Określenie skuteczności przewietrzania drążonych wyrobisk górniczych, których długość nie przekracza 60 metrów przy zastosowaniu wentylatorów wolnostrumieniowych. Gliwice (niepubl.).

REVIEW BY: PROF. DR HAB. INŻ. WACŁAW DZIĘŻYŃSKI, KRAKÓW

Received: 21 June 2003